Space: Science & Technology
A SCIENCE PARTNER JOURNAL

RESEARCH ARTICLE

QoS-Aware Precoding for Dual-Polarized Downlink Massive MIMO LEO Satellite Communications

Yan Huang[1,2], Li You[1,2*], Kezhi Wang[3], and Xiqi Gao[1,2]

[1]National Mobile Communications Research Laboratory, Southeast University, Nanjing 210096, China. [2]Purple Mountain Laboratories, Nanjing 211100, China. [3]Department of Computer Science, Brunel University, London Uxbridge, UK.

*Address correspondence to: lyou@seu.edu.cn

Citation: Huang Y, You L, Wang K, Gao X. QoS-Aware Precoding for Dual-Polarized Downlink Massive MIMO LEO Satellite Communications. *Space Sci. Technol.* 2024;4:Article 0178. https://doi.org/10.34133/space.0178

Submitted 27 December 2023
Revised 29 February 2024
Accepted 7 May 2024
Published 6 November 2024

Low Earth Orbit (LEO) satellite communications (SATCOM) are important for wireless networks and offer better global wireless access services than higher altitude SATCOM options. SATCOM performance is affected by the number of antennas, which is usually constrained by the satellite space. In this paper, the application of dual-polarized technology is considered to assist LEO SATCOM. Compared with single-polarized antennas, dual-polarized antennas utilize two different polarization orientations to transmit and receive data. This can improve the quality of service (QoS) performance, as it allows for twice the amount of data to be transmitted over the same time–frequency resources. Specifically, we characterize the dual-polarized channel in massive multiple-input multiple-output (MIMO) LEO SATCOM and investigate the precoding design for enhancing the system performance. In particular, a precoding optimization problem is formulated, which aims to jointly optimize the system throughput and the QoS performance. We divide the problem into two stages and develop novel algorithms for each stage to obtain the precoding vectors. The numerical results demonstrate that the dual-polarized technology can improve the system throughput, and the proposed algorithm leads to a higher percentage of users achieving their QoS requirements compared to conventional approaches.

Introduction

Low Earth Orbit (LEO) satellite communications (SATCOM) are integral parts of modern space technology [1,2]. They have several advantages over the higher altitude counterparts, including lower latency, faster data transmission rates, and reduced launch costs [3]. As the demands for high-speed internet connectivity and other space-based services continue to grow, LEO SATCOM are expected to play an increasingly important role in shaping the future of the communication systems. The existing works on LEO SATCOM have explored many promising applications. For example, massive multiple-input multiple-output (MIMO) transmission technology has been integrated with LEO SATCOM systems to enhance both spectral efficiency (SE) and energy efficiency (EE) [4–6]. Meanwhile, in [7], the system EE has been considered together with the quality of service (QoS) performance, and the QoS-aware precoding has been studied to enlarge the percentage of users achieving their QoS requirements. Considering the time-varying channels, a user scheduling and power allocation design has been proposed in [8] based on linear precoding, which is capable of ensuring individual QoS requirements within a specific time period. However, SATCOM performance is greatly affected by the number of antennas [9]. Massive MIMO technology can be applied to improve the system performance [10], but the number of antennas is still limited due to the space limitations of the satellite.

Another practical way to improve SATCOM performance is the utilization of dual-polarized antenna arrays with an additional polarization dimension, which effectively doubles the number of parallel subchannels [10]. The model of a 2×2 dual-polarized antennas has been established in [11] and has been generalized for arbitrary array sizes in [12]. Meanwhile, the existence of radiation [13], including the polarization mismatch during the propagation in the scattering environment [10], will affect the dual-polarized antenna performance. Moreover, the compact antenna array faces inherent issues such as mutual coupling effects, which result in energy interchange among elements and impact antenna pattern, impedance characteristics, and reflection coefficients, ultimately affecting system performance positively or negatively [14,15]. To characterize the effects, both the Z-parameter and the S-parameter formulation of the mutual coupling model have been intensively investigated [16]. Many existing works have incorporated the mutual coupling effects in the communication model [17–19].

The dual-polarized antenna array has been extensively applied in various scenarios. In [10], the authors have investigate the performance of dual-polarized technology with the assistance of the reconfigurable intelligent surface in the presence of polarization imperfections. In [20], sub-terahertz bands have employed dual-polarized antennas to handle space occupancy and enhance system SE. Other metrics like EE have also been considered for such systems [21]. These findings inspire the application of this

technique while considering QoS requirements, as each user may require different services with varying QoS requirements [8]. Recent studies have concentrated on maximizing the total throughput of QoS-guaranteed SATCOM, with multiple users requesting network services simultaneously [8]. The max–min fairness optimization framework has been utilized to ensure an acceptable QoS level with dual-polarized SATCOM channels [3]. Furthermore, linear precoding techniques have been utilized to maximize the data throughput in dual-polarized channels [22].

Motivated by the aforementioned considerations, this paper adopts the dual-polarized massive MIMO LEO SATCOM model and focuses on downlink transmission QoS performance. To enhance system throughput, we propose a QoS-aware precoding design for dual-polarized LEO SATCOM channels. The remainder of this paper is organized as follows. We first characterize the time-varying dual-polarized channels in massive MIMO LEO SATCOM. Subsequently, we propose a precoding algorithm with dual-polarized antennas, which can improve QoS performance and system throughput at the same time. The simulation results demonstrate that the dual-polarized technology can improve the system throughput, while the proposed algorithm ensures that more users can achieve their QoS requirements. *Notations:* Column vectors and matrices are typeset in lowercase and uppercase boldface letters, respectively. The $M \times N$ vector space is denoted by $\mathbb{C}^{M\times N}$. The identity matrix of size $M \times M$ is marked by $\mathbf{I}_M$. The Hadamard product is represented by $\odot$. The Kronecker product is denoted by $\otimes$. The operator *det* $\{.\}$ denote the determinant operation. The transpose, conjugate, and conjugate-transpose operations on matrices are denoted by $(.)^T$, $(.)^*$, and $(.)^H$, respectively.

System model and problem formulation

In a dual-polarized massive MIMO LEO SATCOM system downlink, the satellite-side transmitter serves K user terminals (UTs) and is equipped with a dual-polarized uniform planar array (UPA). The UPA has $N_{\mathrm{t}}^{\mathrm{x}}$ and $N_{\mathrm{t}}^{\mathrm{y}}$ dual-polarized elements on the x and y axes, respectively, with half-wavelength separation. The total number of dual-polarized antennas sums up to $N_{\mathrm{t}}^{\mathrm{x}}N_{\mathrm{t}}^{\mathrm{y}}$; thus, the number of polarized antennas is $N_{\mathrm{t}}^{\mathrm{d}} = 2N_{\mathrm{t}}^{\mathrm{x}}N_{\mathrm{t}}^{\mathrm{y}}$. Besides, each UT is assumed to adopt one dual-polarized element.

Dual-polarized massive MIMO LEO SATCOM Downlink Channel

In this subsection, we describe the dual-polarized downlink channel between the satellite and UTs in detail. We assume that the channel $\mathbf{H}_k \in \mathbb{C}^{2\times N_{\mathrm{t}}^{\mathrm{d}}}$ for UT k follows the Rician distribution with Rician factor κ_k, based on which $\mathbf{H}_k$ can be written as

$$\mathbf{H}_k = \left(\sqrt{\frac{\kappa_k\gamma_k}{1+\kappa_k}}\overline{\mathbf{H}}_k + \sqrt{\frac{\gamma_k}{1+\kappa_k}}\widetilde{\mathbf{H}}_k\right)\mathbf{U}(\psi), \tag{1}$$

where γ_k represents the average channel power associated with relative position of the satellite and UT k. The dual polarization effects can be considered and are characterized by the matrix $\mathbf{X}$, which is given by

$$\mathbf{X} = \begin{bmatrix} \sqrt{\frac{\chi}{1+\chi}} & \sqrt{\frac{1}{1+\chi}} \\ \sqrt{\frac{1}{1+\chi}} & \sqrt{\frac{\chi}{1+\chi}} \end{bmatrix}. \tag{2}$$

The parameter χ measures the channel discrimination ability between 2 polarizations, which is known as cross polarization discrimination (XPD) [23].

In Eq. 1, $\overline{\mathbf{H}}_k$ denotes the deterministic line-of-sight (LoS) part of the channel, which is modeled as [12]

$$\overline{\mathbf{H}}_k = \mathbf{X} \otimes \mathbf{v}_k^H \in \mathbb{C}^{2\times N_{\mathrm{t}}^{\mathrm{d}}}, \tag{3}$$

where the UPA response vector for the kth UT can be given by [4].

$$\mathbf{v}_k = \mathbf{v}_k^{\mathrm{x}} \otimes \mathbf{v}_k^{\mathrm{y}} \in \mathbb{C}^{N_{\mathrm{t}}^{\mathrm{x}}N_{\mathrm{t}}^{\mathrm{y}}\times 1}, \tag{4}$$

where $\mathbf{v}_k^x$ and $\mathbf{v}_k^y$ are the array response vectors of the x and y axes, given by

$$\begin{aligned} \mathbf{v}_k^x &\triangleq \mathbf{v}_x\left(\vartheta_k^x\right) = \frac{1}{\sqrt{N_{\mathrm{t}}^x}}\exp\left[\left\{-j\pi\vartheta_k^x\right\}\cdots\exp\left\{-j\pi\left(N_{\mathrm{t}}^x-1\right)\vartheta_k^x\right\}\right]^T \in \mathbb{C}^{N_{\mathrm{t}}^x\times 1}, \\ \mathbf{v}_k^y &\triangleq \mathbf{v}_y\left(\vartheta_k^y\right) = \frac{1}{\sqrt{N_{\mathrm{t}}^y}}\exp\left[\left\{-j\pi\vartheta_k^y\right\}\cdots\exp\left\{-j\pi\left(N_{\mathrm{t}}^y-1\right)\vartheta_k^y\right\}\right]^T \in \mathbb{C}^{N_{\mathrm{t}}^y\times 1}. \end{aligned} \tag{5}$$

The space angles ϑ_k^{x} and ϑ_k^{y} can be calculated using the physical angles θ_k^{x} and θ_k^{y} [4]. Specially, $\vartheta_k^{\mathrm{x}} = \sin\theta_k^{\mathrm{y}}\cos\theta_k^{\mathrm{x}}$ and $\vartheta_k^{\mathrm{y}} = \cos\theta_k^{\mathrm{x}}$ [4].

Meanwhile, the non-line-of-sight (NLoS) part of the channel corresponding to random scattering can be modeled as [12]

$$\widetilde{\mathbf{H}}_k = (\mathbf{X}\odot\mathbf{\Phi})\otimes\left(\widetilde{g}_k\mathbf{v}_k^H\right) \in \mathbb{C}^{2\times N_{\mathrm{t}}^{\mathrm{d}}}, \tag{6}$$

where $\widetilde{g}_k \sim \mathcal{CN}(0,1)$, and $\mathbf{\Phi} \in \mathbb{C}^{2\times 2}$ models the phase shift due to the scattering differences among the 4 polarized channels [24].

In addition, $\mathbf{U}(\psi)$ in Eq. 1 denotes the rotation matrix with respect to a given orientation difference ψ between the dual-polarized antennas at the LEO satellite side and the UT side, which can be defined as follows [25]

$$\mathbf{U}(\psi) = \Psi(\psi)\otimes\mathbf{I}_{N_{\mathrm{t}}^{\mathrm{x}}\times N_{\mathrm{t}}^{\mathrm{y}}} = \begin{bmatrix} \cos\psi & -\sin\psi \\ \sin\psi & \cos\psi \end{bmatrix}\otimes\mathbf{I}_{N_{\mathrm{t}}^{\mathrm{x}}\times N_{\mathrm{t}}^{\mathrm{y}}} \in \mathbb{C}^{N_{\mathrm{t}}^{\mathrm{d}}\times N_{\mathrm{t}}^{\mathrm{d}}}. \tag{7}$$

Based on the above analysis, we set $\widetilde{\mathbf{G}} = \widetilde{g}_k\mathbf{\Phi}$ and reformulate channel $\mathbf{H}_k$ as

$$\begin{aligned} \mathbf{H}_k &= \left[\left(\sqrt{\frac{\kappa_k\gamma_k}{1+\kappa_k}}\mathbf{X} + \sqrt{\frac{\gamma_k}{1+\kappa_k}}\widetilde{g}_k\mathbf{X}\odot\mathbf{\Phi}\right)\otimes\mathbf{v}_k^H\right]\mathbf{U}(\psi) \\ &= \left[\left(\sqrt{\frac{\kappa_k\gamma_k}{1+\kappa_k}}\mathbf{X} + \sqrt{\frac{\gamma_k}{1+\kappa_k}}\mathbf{X}\odot\widetilde{\mathbf{G}}\right)\otimes\mathbf{v}_k^H\right]\mathbf{U}(\psi). \end{aligned} \tag{8}$$

For the dual-polarized UPA, the mutual coupling occurs not only between 2 elements but also between the 2 ports of co- and cross-polarization for each dual-polarized element [26]. Then, we define $\mathbf{\Gamma}_d \in \mathbb{C}^{N_{\mathrm{t}}^{\mathrm{d}}\times N_{\mathrm{t}}^{\mathrm{d}}}$ as the symmetric mutual coupling matrix

of the dual-polarized UPA at the transmitter [27,28]. The downlink channel is modeled as follows

$$\mathbf{H}_k = \left[\left(\sqrt{\frac{\kappa_k\gamma_k}{1+\kappa_k}}\mathbf{X} + \sqrt{\frac{\gamma_k}{1+\kappa_k}}\mathbf{X}\odot\widetilde{\mathbf{G}}\right)\otimes\mathbf{v}_k^H\right]\boldsymbol{\Gamma}_d\mathbf{U}(\psi)\cdot \quad (9)$$

Upper bound of the ergodic rate

At time t, the satellite sends data signals to the users scheduled to receive them. The received signal of the kth UT, denoted by $\mathbf{y}_k(t)$, is expressed as

$$\begin{aligned}\mathbf{y}_k(t) &= \mathbf{H}_k(t)\sum_{\ell=1}^{K}\mathbf{b}_\ell(t)s_\ell(t)+\mathbf{n}_k(t)\\ &= \mathbf{H}_k(t)\mathbf{b}_k(t)s_k(t)+\mathbf{H}_k(t)\sum_{\ell\neq k}\mathbf{b}_\ell(t)s_\ell(t)+\mathbf{n}_k(t)\in\mathbb{C}^{2\times 1}.\end{aligned} \quad (10)$$

In Eq. 10, $s_k(t)$ is the transmit signal for user k with $|s_k(t)|^2=1$, $\mathbf{n}_k(t)\in\mathbb{C}^{2\times 1}$ is the additive white Gaussian noise with average energy N_0, and $\mathbf{b}_k(t)\in\mathbb{C}^{N_t^d\times 1}$ represents the precoding vectors of user k. Precoding vectors are limited by the satellite's power budget, which can be expressed as

$$\sum_{k=1}^{K}\left\|\mathbf{b}_k(t)\right\|_2^2\le P_{\text{tot}},\ \forall t, \quad (11)$$

where P_{tot} is the maximum transmit power that the satellite can allocate.

Next, we consider the transmission rate expression based on Eq. 10. The right-hand side of Eq. 10 consists of two parts. The first part shows the desired signal, and the second part displays the interference from other users. Based on the aforementioned analysis, the data throughput for the kth user at time t can be expressed as follows

$$R_k(t) = B_w\log\det\left(\mathbf{I}_2+\mathbf{C}^{-1}(t)\mathbf{H}_k(t)\mathbf{b}_k(t)\mathbf{b}_k^H(t)\mathbf{H}_k^H(t)\right). \quad (12)$$

where $\mathbf{C}(t)=\sum_{\ell\neq k}\mathbf{H}_k(t)\mathbf{b}_\ell(t)\mathbf{b}_\ell^H(t)\mathbf{H}_k^H(t)+N_0\mathbf{I}_2$, and B_w is the system bandwidth.

Note that the channel state information (CSI) varies over time, and its acquisition accuracy is critical for the performance. Considering the pilot training and channel estimation overhead, obtaining the instantaneous CSI (iCSI) at the satellite side is challenging [29]. Thus, we propose a precoding design based on the statistical CSI (sCSI) knowledge χ, κ_k, γ_k, $\Psi(\psi)$ and $\mathbf{v}_k$. It can be noted that the sCSI can remain stable for extended periods [30]. In this paper, we assume that the sCSI remains unchanged in the continuous time set $\bar{t}$ if $\left\|\mathbf{v}_k(t_0)-\mathbf{v}_k(t_1)\right\|_2^2\le 0.02*\left\|\mathbf{v}_k(t_0)\right\|_2^2,\ \forall t_0,t_1\in\bar{t}$, and define it as a time block. After that, the statistical channel information will change accordingly based on Eqs. 4 and 5. We consider the ergodic data rate with sCSI. Based on the above transmission model, the ergodic data rate at time block $\bar{t}$ is given by

$$R_k(\bar{t}) = B_w\mathbb{E}_{t\in\bar{t}}\left\{\log\det\left(\mathbf{I}_2+\mathbf{C}^{-1}(t)\mathbf{H}_k(t)\mathbf{b}_k(t)\mathbf{b}_k^H(t)\mathbf{H}_k^H(t)\right)\right\}, \quad (13)$$

where $\mathbb{E}$ represents the expectation operator and R_k remains unchanged in time block $\bar{t}$ with constant $\mathbf{b}_k(t), t\in\bar{t}$.

The value $R_k(\bar{t})$ can be estimated via Monte Carlo method, but it will lead to high computational complexity. Next, we consider deriving a tight upper bound of the ergodic rate based on the sCSI [31]. First, we rewrite the expression as

$$\begin{aligned}R_k(\bar{t}) &= B_w\mathbb{E}_{t\in\bar{t}}\left\{\log\det\mathbf{C}^{-1}(t)\left(\mathbf{C}(t)+\mathbf{H}_k(t)\mathbf{b}_k(t)\mathbf{b}_k^H(t)\mathbf{H}_k^H(t)\right)\right\}\\ &= B_w\mathbb{E}_{t\in\bar{t}}\left\{\log\det\left(N_0\mathbf{I}_{N_t^d}+\sum_{\ell=1}^{K}\mathbf{b}_\ell(t)\mathbf{b}_\ell^H(t)\mathbf{H}_k^H(t)\mathbf{H}_k(t)\right)\right\}\\ &\quad - B_w\mathbb{E}_{t\in\bar{t}}\left\{\log\det\left(\sum_{\ell\neq k}\mathbf{b}_\ell(t)\mathbf{b}_\ell^H(t)\mathbf{H}_k^H(t)\mathbf{H}_k(t)+N_0\mathbf{I}_{N_t^d}\right)\right\}.\end{aligned} \quad (14)$$

Note that $R_k(\bar{t})$ is concave with respect to the matrix $\mathbf{H}_k^H(t)\mathbf{H}_k(t)$. Thus, the upper bound can be written as

$$\begin{aligned}R_k(\bar{t})\le\overline{R}_k(\bar{t}) = {} & B_w\log\det\left(N_0\mathbf{I}_{N_t^d}+\sum_{\ell=1}^{K}\mathbf{b}_\ell(\bar{t})\mathbf{b}_\ell^H(\bar{t})\mathbb{E}_{t\in\bar{t}}\left\{\mathbf{H}_k^H(t)\mathbf{H}_k(t)\right\}\right)\\ & - B_w\log\det\left(N_0\mathbf{I}_{N_t^d}+\sum_{\ell\neq k}\mathbf{b}_\ell(\bar{t})\mathbf{b}_\ell^H(\bar{t})\mathbb{E}_{t\in\bar{t}}\left\{\mathbf{H}_k^H(t)\mathbf{H}_k(t)\right\}\right),\end{aligned} \quad (15)$$

where the expectation expression $\mathbb{E}_{t\in\bar{t}}\left\{\mathbf{H}_k^H(t)\mathbf{H}_k(t)\right\}$ represents the channel correlation matrix at the satellite side for the kth UT, given by

$$\begin{aligned}\mathbb{E}_{t\in\bar{t}}\left\{\mathbf{H}_k^H(t)\mathbf{H}_k(t)\right\} &= \boldsymbol{\Gamma}_d^T\mathbf{U}^T(\psi)\left(\frac{\kappa_k\gamma_k}{1+\kappa_k}\mathbf{X}^H\mathbf{X}+\frac{\gamma_k}{1+\kappa_k}\right)\otimes\mathbf{v}_k(\bar{t})\mathbf{v}_k^H(\bar{t})\mathbf{U}(\psi)\boldsymbol{\Gamma}_d\\ &= \boldsymbol{\Gamma}^T\mathbf{U}^T(\psi)\left[\mathbf{D}\otimes\mathbf{v}_k(\bar{t})\mathbf{v}_k^H(\bar{t})\right]\mathbf{U}(\psi)\boldsymbol{\Gamma},\end{aligned} \quad (16)$$

where $\mathbf{D}$ is a real symmetric matrix given by

$$\mathbf{C} = \frac{\kappa_k\gamma_k}{1+\kappa_k}\mathbf{X}^H\mathbf{X}+\frac{\gamma_k}{1+\kappa_k}\mathbf{I}_2 = \begin{bmatrix}\gamma_k & \frac{2\sqrt{\chi}}{1+\chi}\frac{\kappa_k\gamma_k}{1+\kappa_k}\\ \frac{2\sqrt{\chi}}{1+\chi}\frac{\kappa_k\gamma_k}{1+\kappa_k} & \gamma_k\end{bmatrix}. \quad (17)$$

If we define

$$\boldsymbol{\Sigma} = \begin{bmatrix}\gamma_k+\frac{2\sqrt{\chi}}{1+\chi}\frac{\kappa_k\gamma_k}{1+\kappa_k} & 0\\ 0 & \gamma_k-\frac{2\sqrt{\chi}}{1+\chi}\frac{\kappa_k\gamma_k}{1+\kappa_k}\end{bmatrix},\ \mathbf{Q} = \begin{bmatrix}\frac{1}{\sqrt{2}} & \frac{1}{\sqrt{2}}\\ \frac{1}{\sqrt{2}} & -\frac{1}{\sqrt{2}}\end{bmatrix}, \quad (18)$$

then $\mathbf{D}$ can be decomposed as $\mathbf{D}=\mathbf{Q}\boldsymbol{\Sigma}\mathbf{Q}^T$. Thus, we have $\mathbb{E}_{t\in\bar{t}}\left\{\mathbf{H}_k^H(t)\mathbf{H}_k(t)\right\}=\overline{\mathbf{H}}_k^H(\bar{t})\overline{\mathbf{H}}_k(\bar{t})$, where

$$\overline{\mathbf{H}}_k(\bar{t}) = \left[\boldsymbol{\Sigma}^{\frac{1}{2}}\mathbf{Q}^T\Psi(\psi)\otimes\mathbf{v}_k^H(\bar{t})\right]\boldsymbol{\Gamma}. \quad (19)$$

Note that the required CSI knowledge is assumed to be invariant when the distance traveled by the satellite is within 2% of the distance between the satellite and the UTs. It can be updated accordingly with large variations of the channel [4] based on Eq. 4 and 5. Subsequently, $\overline{R}_k$ can be rewritten as

$$\overline{R}_k(\bar{t}) = B_w\log\det\left(\mathbf{I}_2+\overline{\mathbf{C}}(\bar{t})^{-1}\overline{\mathbf{H}}_k(\bar{t})\mathbf{b}_k(\bar{t})\mathbf{b}_k^H(\bar{t})\overline{\mathbf{H}}_k^H(\bar{t})\right), \quad (20)$$

where $\overline{\mathbf{C}}(\bar{t}) = \sum_{\ell \neq k} \overline{\mathbf{H}}_k(\bar{t}) \mathbf{b}_\ell(\bar{t}) \mathbf{b}_\ell^H(\bar{t}) \overline{\mathbf{H}}_k^H(\bar{t}) + N_0 \mathbf{I}_2$.

Problem formulation

In this paper, we consider optimizing the total data throughput of the LEO SATCOM. The throughput of user k in T time blocks can be expressed as

$$Q_k = \sum_{\bar{t}=1}^{T} \overline{R}_k(\bar{t}), \tag{21}$$

where $\overline{R}_k(\bar{t})$ is the upper bound of the ergodic rate based on the slow-varying sCSI $\overline{\mathbf{H}}_k$ given in Eq. 20.

In the downlink transmission, different services have different delay constraints. We assume that user k requests to transmit $Q_k^{\min}$ in τ_k time blocks, with the unit being Mbits. Then, from Eq. 21, we get $Q_k = \sum_{(\bar{t})=1}^{\tau_k} \overline{R}_k(\bar{t})$. If $Q_k \geq Q_k^{\min}$, then the QoS requirement cannot be satisfied. The throughput successfully delivered to user k is given by

$$G_k = Q_k \cdot \mathbf{1}\left(Q_k \geq Q_k^{\min}\right), \tag{22}$$

where $\mathbf{1}(\cdot)$ is the indicator function.

In this work, we aim to optimize the successfully delivered throughput over the selected time blocks, subject to individual delay constraints. We denote $\mathbf{b} = \{\mathbf{b}_k(\bar{t}), \forall \mathrm{t}, \forall \mathrm{k}\}$. The precoding problem is formulated as follows

$$\begin{aligned} \mathcal{P}_1: \underset{\mathbf{b}}{\text{maximize}} \quad & \sum_{k=1}^{K} G_k \\ \text{s. t.} \quad & (11), (22). \end{aligned} \tag{23}$$

It can be noted that $\mathcal{P}_1$ is a fractional nonconvex problem, which presents a challenge. In the following sections, we will propose a precoding design for the dual-polarized LEO SATCOM channels.

Precoding Algorithm

Note that $\mathcal{P}_1$ involves nonconvex constraints and discontinuous constraints. In addition, the resource allocation process also involves user scheduling, which makes it challenging to handle. In this section, we present a 2-stage algorithm for addressing $\mathcal{P}_1$, which aims to enhance the QoS performance and optimize the successfully delivered throughput in dual-polarized LEO SATCOM channels at the same time. In stage I, we maximize the number of users who can achieve their QoS requirements. Then, in stage II, we allocate time blocks for the selected users from stage I, while the precoding vectors are optimized to maximize the throughput.

Specifically, in stage I, we split $\mathcal{K}$ into two groups. $\mathcal{S}$ includes users who can achieve their QoS requirements, while the others are in $\mathcal{K} \setminus \mathcal{S}$. The problem in the first stage can be written as

$$\begin{aligned} \mathcal{P}_2: \underset{\mathbf{b}, \mathcal{S}}{\text{maximize}} \quad & |\mathcal{S}| \\ \text{s. t.} \quad & (11), \\ & \mathcal{S} \subseteq \mathcal{K}, \\ & \sum_{\bar{t}=1}^{\tau_k} \overline{R}_k(\bar{t}) \geq Q_k^{\min}, \ \forall k \in \mathcal{S}. \end{aligned} \tag{24}$$

Methods for handling problem $\mathcal{P}_2$ will be given in the later sections. Based on the results in Eq. 24, we proceed with the precoding matrices across all time blocks in stage II, aimed at maximizing the successfully delivered throughput. This optimization problem can be formulated as follows

$$\begin{aligned} \mathcal{P}_3: \underset{\{\mathbf{b}_k(\bar{t})\}_{k \in \mathcal{S}}}{\text{maximize}} \quad & \sum\nolimits_{k \in \mathcal{S}} \overline{Q}_k \\ \text{s. t.} \quad & (11), \\ & \sum\nolimits_{\bar{t}=1}^{\tau_k} \overline{R}_k(\bar{t}) \geq Q_k^{\min}, \ \forall k \in \mathcal{S}. \end{aligned} \tag{25}$$

The optimization problems in the 2 stages of the proposed system are computationally challenging to handle due to their nonconvex nature [32]. Exhaustive search is an intuitive approach. For instance, to maximize the throughput, one needs to obtain the precoding matrices for every possible time block allocation scheme and user scheduling scheme and then obtain the corresponding objective value. The optimal solution is then obtained by selecting the time block allocation scheme that achieves the maximum throughput, along with the corresponding precoding matrices. However, the exponential growth of the complexity of exhaustive search with the number of time blocks and number of users makes it impractical. Hence, alternative algorithms need to be developed to handle these 2 problems.

Stage I: User selection algorithm

We propose a user selection algorithm in this subsection to ensure the QoS level for the majority of users. This approach involves constructing an alternative problem by introducing auxiliary variables $\{\alpha_k\}_{k \in \mathcal{S}}$ for an arbitrary subset of users, $\mathcal{S}$ [32], as detailed below

$$\mathcal{P}_4: \quad \underset{\{\mathbf{b}_k(\bar{t})\}_{k \in \mathcal{S}}, \{\alpha_k\}_{k \in \mathcal{S}}}{\text{minimize}} \quad \sum_{k \in \mathcal{S}} \left(\alpha_k - 1\right)^2 \tag{26a}$$

$$\text{s. t.} \quad (11), \quad \sum_{\bar{t}=1}^{\tau_k} \overline{R}_k(\bar{t}) \geq \alpha_k^2 Q_k^{\min}, \ \forall k \in \mathcal{S}. \tag{26b}$$

It is obvious that the optimal α_k should satisfy that $\alpha_k \leq 1$. In addition, it is worth noting that the QoS requirement for a user k can be fulfilled if and only if the optimal $\alpha_k = 1$. Consequently, the problem of maximizing the number of users whose QoS requirements are satisfied can be rephrased as identifying the largest subset of users $\mathcal{S}$ such that the optimal $\alpha_k = 1, \forall k \in \mathcal{S}$.

Next, we propose a user selection algorithm to handle $\mathcal{P}_4$. The algorithm removes one user with the smallest $\alpha_k \leq 1$ in each iteration, as this user has the largest difference in QoS. This approach is intuitive and reasonable based on the above analysis.

In step 3 of Algorithm 1, we encounter the nonconvex optimization problem, which poses significant challenge. In order to address this issue, we leverage the Lagrange dual transform to reformulate the problem. The Lagrange dual transform [33] enables us to replace fractional expressions with corresponding parameters from an auxiliary variable collection and manipulate the ratio outside the logarithmic operator. This approach not only facilitates the optimization process but also provides insights into the problem structure and enables us to derive analytical solutions.

Algorithm 1 User Selection Algorithm for $\mathcal{P}_2$

Input: Initialize the subset $\mathcal{S}=\{1,2,\ldots,K\}$, and $k^*=0$.
1: **repeat**
2: Remove user k^* and update $\mathcal{S}=\mathcal{S}\backslash k^*$.
3: With the given $\mathcal{S}$, update $\{\alpha_k\}_{k\in\mathcal{S}}$ and $\{\mathbf{b}_k(\bar{t})\}_{k\in\mathcal{S}}$ via $\mathcal{P}_4$.
4: Update $k^*=\arg\min_{k\in\mathcal{S}}\alpha_k$.
5: **until** $\alpha_k=1,\ \forall k\in\mathcal{S}$.
Output: The optimal subset $\mathcal{S}$.

In particular, with index n, we introduce a set of auxiliary matrices $\{\boldsymbol{\gamma}_k^n(\bar{t})\}_{k\in\mathcal{S}}\in\mathbb{C}^{2\times1}, n=1,2,\ldots$. Then, a set of auxiliary subproblems are introduced to ensure convergence to the globally optimal point of problem $\mathcal{P}_5$. The nth subproblem is given by

$$\mathcal{P}_5^n:\ \underset{\{\mathbf{b}_k^n(\bar{t})\}_{k\in\mathcal{S}},\{\alpha_k^n\}_{k\in\mathcal{S}},\{\boldsymbol{\gamma}_k^n(\bar{t})\}_{k\in\mathcal{S}}}{\text{minimize}}\ \sum_{k\in\mathcal{S}}\left(\alpha_k^n-1\right)^2 \tag{27a}$$

$$\text{s.t.}\ \ (11),\ \ f(\{\mathbf{b}_k^n(\bar{t})\}_{k\in\mathcal{S}},\{\alpha_k^n\}_{k\in\mathcal{S}},\boldsymbol{\gamma}_k^n(\bar{t}))\geq\frac{\alpha_k^2Q_k^{\min}}{B_w},\forall k\in\mathcal{S}, \tag{27b}$$

where

$$\begin{aligned}f=&\sum_{\bar{t}=1}^{\tau_k}\left(\log\det\left(\mathbf{I}_2+\boldsymbol{\gamma}_k^n(\bar{t})\right)-\det\left(\boldsymbol{\gamma}_k^n(\bar{t})\right)\right.\\&+\det\left(\left\{\sum\nolimits_{\ell\in\mathcal{S}}\overline{\mathbf{H}}_k(\bar{t})\mathbf{b}_\ell(\bar{t})\mathbf{b}_\ell^H(\bar{t})\overline{\mathbf{H}}_k^H(\bar{t})+N_0\mathbf{I}_2\right\}^{-1}\right.\\&\left.\left.\left\{\left(\mathbf{I}_2+\boldsymbol{\gamma}_k^n(\bar{t})\right)\overline{\mathbf{H}}_k(\bar{t})\mathbf{b}_k(\bar{t})\mathbf{b}_k^H(\bar{t})\overline{\mathbf{H}}_k^H(\bar{t})\right\}\right)\right).\end{aligned} \tag{28}$$

An alternating optimization framework is used to iteratively optimize the parameters of the subproblems. When $\{\mathbf{b}_k^n(\bar{t})\}_{k\in\mathcal{S}}$ and $\{\alpha_k^n\}_{k\in\mathcal{S}}$ are fixed, the optimal $\{\boldsymbol{\gamma}_k^n(\bar{t})\}_{k\in\mathcal{S}}$ can be achieved when their first-order derivatives in Eq. 30 are all equal to zero, which is given by

$$\boldsymbol{\gamma}_k^n(\bar{t})=\left(\sum_{\ell\neq k}\overline{\mathbf{H}}_k(\bar{t})\mathbf{b}_\ell(\bar{t})\mathbf{b}_\ell^H(\bar{t})\overline{\mathbf{H}}_k^H(\bar{t})+N_0\mathbf{I}_2\right)^{-1}\left(\overline{\mathbf{H}}_k(\bar{t})\mathbf{b}_k(\bar{t})\mathbf{b}_k^H(\bar{t})\overline{\mathbf{H}}_k^H(\bar{t})\right). \tag{29}$$

Next, we focus on the optimization of $\{\{\mathbf{b}_k^n(\bar{t})\}_{k\in\mathcal{S}},\{\alpha_k^n\}_{k\in\mathcal{S}}\}$ with fixed $\{\boldsymbol{\gamma}_k^n(\bar{t})\}_{k\in\mathcal{S}}$. Note that $\mathcal{P}_5^n$ is still nonconvex due to the fractional term in Eq. 29. Then, we apply the quadratic transform [32]. We introduce the set of auxiliary variables $\{y_k^n(\bar{t})\}_{k\in\mathcal{S}}$ for each problem $\mathcal{P}_5^n$, and the constraint in Eq. 29 can be transformed into

$$\begin{aligned}&\sum\nolimits_{\bar{t}=1}^{\tau_k}\left(\log\det(\mathbf{I}_2+\boldsymbol{\gamma}_k^n(\bar{t}))-\det(\boldsymbol{\gamma}_k^n(\bar{t}))\right.\\&+2y_k^n(\bar{t})\sqrt{\det\left((\mathbf{I}_2+\boldsymbol{\gamma}_k^n(\bar{t}))\overline{\mathbf{H}}_k(\bar{t})\mathbf{b}_k(\bar{t})\mathbf{b}_k^H(\bar{t})\overline{\mathbf{H}}_k^H(\bar{t})\right)}\\&\left.-(y_k^n(\bar{t}))^2N_0-\sum\nolimits_{\ell\in\mathcal{S}}\det\left(\overline{\mathbf{H}}_k(\bar{t})\mathbf{b}_\ell(\bar{t})\mathbf{b}_\ell^H(\bar{t})\overline{\mathbf{H}}_k^H(\bar{t})\right)\right)\geq\frac{\alpha_k^2Q_k^{\min}}{B_w},\forall k\in\mathcal{S}.\end{aligned} \tag{30}$$

Thus, we equivalently consider the following problem

$$\mathcal{P}_6^n:\ \underset{\{\mathbf{b}_k^n(\bar{t})\}_{k\in\mathcal{S}},\{\alpha_k^n\}_{k\in\mathcal{S}},\{\boldsymbol{\gamma}_k^n(\bar{t})\}_{k\in\mathcal{S}},\{y_k^n(\bar{t})\}_{k\in\mathcal{S}}}{\text{minimize}}\ \sum\nolimits_{k\in\mathcal{S}}\left(\alpha_k^n-1\right)^2$$
$$\text{s.t.}\qquad (11),(30). \tag{31}$$

We aim to iteratively optimize $\{\boldsymbol{\gamma}_k^n(\bar{t})\}_{k\in\mathcal{S}}$ and other variables according to Eq. 33. The update of $\{\boldsymbol{\gamma}_k^n(\bar{t})\}_{k\in\mathcal{S}}$ is outlined in Eq. 31. For the optimal $\{y_k^n(\bar{t})\}_{k\in\mathcal{S}}$, the derivative of each $y_k^n(\bar{t})$ in Eq. 32 is calculated and equated to zero, while all other variables are kept fixed, which is given by

$$y_k^n(\bar{t})=\frac{\sqrt{\det\left((\mathbf{I}_2+\boldsymbol{\gamma}_k^n(\bar{t}))\overline{\mathbf{H}}_k(\bar{t})\mathbf{b}_k(\bar{t})\mathbf{b}_k^H(\bar{t})\overline{\mathbf{H}}_k^H(\bar{t})\right)}}{\det\left(\sum\nolimits_{\ell\in\mathcal{S}}\overline{\mathbf{H}}_k(\bar{t})\mathbf{b}_\ell(\bar{t})\mathbf{b}_\ell^H(\bar{t})\overline{\mathbf{H}}_k^H(\bar{t})+N_0\mathbf{I}_2\right)}. \tag{32}$$

Next, we only need to find the optimal $\{\mathbf{b}_k^n(\bar{t})\}_{k\in\mathcal{S}}$ and $\{\alpha_k^n\}_{k\in\mathcal{S}}$, which is listed as follows

$$\mathcal{P}_7^n:\ \underset{\{\mathbf{b}_k^n(\bar{t})\}_{k\in\mathcal{S}},\{\alpha_k^n\}_{k\in\mathcal{S}}}{\text{minimize}}\ \sum\nolimits_{k\in\mathcal{S}}\left(\alpha_k^n-1\right)^2$$
$$\text{s.t.}\qquad (2),(30). \tag{33}$$

Note that with other variables fixed, $\mathcal{P}_7^n$ is a convex problem with cone constraints. Algorithm 2 formally describes an iterative algorithm to handle it, which is a second-order cone programming (SOCP) problem that can be optimally solved using existing techniques, such as the interior-point method [30]. The initial α_k is set as 0 for each user so that the initial $\mathbf{b}_k(t)$ only needs to satisfy Eq. 11. The convergence analysis will be given in the later subsections.

Algorithm 2 Gradient Descent Method for Problem $\mathcal{P}_6^n$

Input: Iterative number $n=1$, the maximum number of iterations $n_{\max}$, the precoding vectors $\{\mathbf{b}_k^1(\bar{t})\}_{k\in\mathcal{S}}$ such that (11) and (26b) are satisfied.
1: **repeat**
2: Calculate $\{\gamma_k^n(\bar{t})\}_{k\in\mathcal{S}}$ via (29).
3: Calculate $\{y_k^n(\bar{t})\}_{k\in\mathcal{S}}$ via (32).
4: With $\{\gamma_k^n(\bar{t})\}_{k\in\mathcal{S}}$ and $\{y_k^n(\bar{t})\}_{k\in\mathcal{S}}$, update $\{\mathbf{b}_k^n(\bar{t})\}_{k\in\mathcal{S}}$ and $\{\alpha_k^n\}_{k\in\mathcal{S}}$ via SOCP problem $\mathcal{P}_7^n$.
5: $n=n+1$.
6: **until** $n=n_{\max}$.
Output: The optimal $\{\alpha_k\}_{k\in\mathcal{S}}=\{\alpha_k^n\}_{k\in\mathcal{S}}$.

Stage II: Throughput optimizing algorithm

We propose an algorithm to handle $\mathcal{P}_3$ in this subsection with the user selection obtained from the "Stage I: User selection algorithm" section. Specifically, we utilize the weighted minimum mean-square error (WMMSE) method [32] and employ the block coordinate descent method [32] to reformulate the original optimization problem as a sequence of subproblems. In each iteration, one of the subproblems involves the optimization of the precoding matrices.

To overcome the challenge of the sum-of-logarithms term with a fractional expression in each logarithmic operator in $\mathcal{P}_3$, we leverage the connections between WMMSE and the rate expression.

First, we consider the linear receiver filter as follows

$$\bar{s}_k(\bar{t}) = \mathbf{u}_k^H(\bar{t})\mathbf{y}_k(\bar{t}), \quad \forall k \in \mathcal{S}. \tag{34}$$

The mean-square error of data transmission of the kth user at the tth time block is calculated by using the receiver filter $\mathbf{u}_k(\bar{t}) \in \mathbb{C}^{2\times 1}$ of the user k and considering the mutual independence of signal vectors and noise, which is expressed as follows

$$\begin{aligned}\mathcal{P}_9: \quad & \underset{\{\mathbf{b}_k(\bar{t})\}_{k\in\mathcal{S}}}{\text{minimize}} \quad \sum\nolimits_{k\in\mathcal{S}} \sum\nolimits_{\bar{t}=1}^{\tau_k} w_k(\bar{t}) e_k(\bar{t}) \\ \text{s.t.} \quad & (11), \ \sum\nolimits_{\bar{t}=1}^{\tau_k} w_k(\bar{t}) e_k(\bar{t}) \le \sum\nolimits_{\bar{t}=1}^{\tau_k} \left(\log w_k(\bar{t}) + 1\right) - \frac{Q_k^{\min}}{B_{\mathrm{w}}}, \ \forall k \in \mathcal{S}.\end{aligned} \tag{35}$$

Next, we introduce a set of auxiliary variables $\{w_k(\bar{t})\}_{k\in\mathcal{S}}$ for the tth time block and define the following functions [32]

$$r_k(\bar{t}) = B_{\mathrm{w}}\left(\log w_k(\bar{t}) - w_k(\bar{t}) e_k(\bar{t}) + 1\right), \quad \forall k \in \mathcal{S}\cdot \tag{36}$$

Meanwhile, with given $\{\mathbf{b}_k(\bar{t})\}_{k\in\mathcal{S}}$, $r_k(\bar{t})$ is the lower bound of the rate expression in Eq. 20. Note that when the other two are fixed, $r_k(\bar{t})$ is a concave for $\{\mathbf{b}_k(\bar{t})\}_{k\in\mathcal{S}}$, $\{\mathbf{u}_k(\bar{t})\}_{k\in\mathcal{S}}$, and $\{w_k(\bar{t})\}_{k\in\mathcal{S}}$. Specially, the optimal $\{\mathbf{u}_k(\bar{t})\}_{k\in\mathcal{S}}$ and $\{w_k(\bar{t})\}_{k\in\mathcal{S}}$ is given by

$$\mathbf{u}_k(\bar{t}) = \left(\sum_{i\in\mathcal{S}} \left(\overline{\mathbf{H}}_k(\bar{t})\mathbf{b}_i(\bar{t})\right)\left(\overline{\mathbf{H}}_k(\bar{t})\mathbf{b}_i(\bar{t})\right)^H + N_0\mathbf{I}\right)^{-1} \overline{\mathbf{H}}_k(\bar{t})\mathbf{b}_k(\bar{t}) \in \mathbb{C}^{2\times 1}, \ \forall k \in \mathcal{S}. \tag{37a}$$

$$w_k(\bar{t}) = \left(e_k(\bar{t})\right)^{-1}, \ \forall k \in \mathcal{S}. \tag{37b}$$

where $e_k(\bar{t})$ in Eq. 37b is obtained by plugging Eq. 37a into Eq. 35. We use $r_k(\bar{t})$ to replace the rate expression in $\mathcal{P}_3$ and introduce the index m; the problem is transformed as follows

$$\begin{aligned}\mathcal{P}_8^m: \quad & \underset{\{\mathbf{b}_k^m(\bar{t})\}_{k\in\mathcal{S}}, \{\mathbf{u}_k^m(\bar{t})\}_{k\in\mathcal{S}}, \{w_k^m(\bar{t})\}_{k\in\mathcal{S}}}{\text{maximize}} \quad \sum\nolimits_{k\in\mathcal{S}} \widetilde{Q}_k \\ \text{s.t.} \quad & (11), \\ & \widetilde{Q}_k = \sum\nolimits_{\bar{t}=1}^{\tau_k} r_k(\bar{t}), \ \forall k \in \mathcal{S}, \\ & \widetilde{Q}_k \ge Q_k^{\min}, \ \forall k \in \mathcal{S}.\end{aligned} \tag{38}$$

Next, the block coordinate descent method [32] is applied. Specially, we optimize the 3 sets of variables in $\mathcal{P}_8^m$ iteratively. With given $\{\mathbf{b}_k^m(\bar{t})\}_{k\in\mathcal{S}}$, $\{\mathbf{u}_k^m(\bar{t})\}_{k\in\mathcal{S}}$ and $\{w_k^m(\bar{t})\}_{k\in\mathcal{S}}$ can be optimized via Eqs. 37a and 37b, respectively. Next, we focus on the optimization of the precoding matrices.

For convenience, we omit the iterative number in the block coordinate descent method and remove the irrelevant terms. The problem turns into

$$\begin{aligned}\mathcal{P}_9: \quad & \underset{\{\mathbf{b}_k(\bar{t})\}_{k\in\mathcal{S}}}{\text{minimize}} \quad \sum\nolimits_{k\in\mathcal{S}} \sum\nolimits_{\bar{t}=1}^{\tau_k} w_k(\bar{t}) e_k(\bar{t}) \\ \text{s.t.} \quad & (11), \ \sum\nolimits_{\bar{t}=1}^{\tau_k} w_k(\bar{t}) e_k(\bar{t}) \le \sum\nolimits_{\bar{t}=1}^{\tau_k} \left(\log w_k(\bar{t}) + 1\right) - \frac{Q_k^{\min}}{B_{\mathrm{w}}}, \ \forall k \in \mathcal{S}.\end{aligned} \tag{39}$$

Since $e_k(\bar{t})$ is a quadratic function of $\{\mathbf{b}_k(\bar{t})\}_{k\in\mathcal{S}}$, $\mathcal{P}_9$ is a convex problem with cone constraints. Algorithm 3 formally describes an iterative algorithm to handle it, which is an SOCP problem that can be optimally solved using existing techniques, such as the interior-point method [30].

Algorithm 3 Block Alternating Optimization for $\mathcal{P}_3$

Input: Iterative number $m = 1$, the maximum number of iterations $m_{\max}$, user selection $\mathcal{S}$ based on Stage I, the precoding vectors $\{\mathbf{b}_k^1(\bar{t})\}_{k\in\mathcal{S}}$ such that constraints in (25) are satisfied.

1: **repeat**
2: Calculate $\{\mathbf{u}_k^m(\bar{t})\}_{k\in\mathcal{S}}$ via (37a).
3: Calculate $\{w_k^m(\bar{t})\}_{k\in\mathcal{S}}$ via (37b).
4: With $\{\mathbf{u}_k^m(\bar{t})\}_{k\in\mathcal{S}}$ in Step 2 and $\{w_k^m(\bar{t})\}_{k\in\mathcal{S}}$, update $\{\mathbf{b}_k^m(\bar{t})\}_{k\in\mathcal{S}}$ via SOCP problem $\mathcal{P}_9$.
5: **until** $m = m_{\max}$.

Output: The optimal $\{\mathbf{b}_k(\bar{t})\}_{k\in\mathcal{S}} = \{\mathbf{b}_k^m(\bar{t})\}_{k\in\mathcal{S}}$.

Convergence and computational complexity analysis

In stage I, it can be observed that Algorithm 2 involves the Lagrange dual transform and the interior-point method. It is demonstrated in [33] that the Lagrange dual transform is guaranteed to converge, with the weighted sum rate monotonically nondecreasing after each iteration. Next, we analyze the complexity of Algorithm 2. Assuming equal candidate sizes for each user, the main complexity of Algorithm 2 lies in step 3. Specifically, it is step 4 in Algorithm 2 that requires handling of the SOCP problem in each iteration. This problem has $\mathcal{O}(\tau_k K + K)$ variables and $\mathcal{O}(\tau_k K + K)$ constraints. From [30], the complexity of each iteration is, $\mathcal{O}\left((\tau_k K + K)^3\right)$ and the number of iterations is $\mathcal{O}\left(\sqrt{\tau_k K + K}\right)$, so the total complexity can be given by $\mathcal{O}\left(K(\tau_k K + K)^{3.5}\right)$.

In stage II, it is worth noting that Algorithm 3 is composed of the WMMSE method and the interior-point method. It has been shown in [32] that the WMMSE method will always converge. We also analyze the computational complexity of Algorithm 3 by assuming identical candidate sizes for each user [32]. The primary computational complexity in each iteration of Algorithm 3 comes from the SOCP problem in step 4. Since the input relies on the result of stage I, we assume that the problem has $\mathcal{O}(N_2)$ variables and $\mathcal{O}(M_2)$ constraints. From [30], the complexity is $\mathcal{O}(N_2^2 M_2)$, and we assume a number of iterations, denoted as N_D. The total complexity is given by $\mathcal{O}(N_D N_2^{2.5} M_2)$.

Simulation results

We present simulation results to evaluate the proposed algorithms' performance in this section, using parameters detailed in the system model in [23]. The simulation operates in the Ka-band, and we provide relevant parameters in Table 1 [23].

According to [29], the downlink channel power can be calculated as follows

$$\gamma_k = G_{\text{sat}} G_{\text{ut}} N_{\text{t}} \left(\frac{c}{4\pi f_{\text{c}} d_0} \right)^2, \forall k. \tag{40}$$

where G_{sat} and G_{ut} represent the antenna gains of the transmitter and the receiver, respectively. The noise power, denoted by N_0, is defined as $k_{\text{B}} \Delta_B T_{\text{n}}$, with k_{B} being the Boltzmann constant and $T_{\text{n}} = 300$ K being the noise temperature [29].

In stage I, the cardinality of the object function S decreases after each iteration, so the iterations will always converge, thus is omitted. In stage II, the iterative process is shown in Fig. 1. Note that it converges rapidly for different power budgets.

Next, we conduct simulations to compare the performance of the proposed algorithm under different XPD values in dual-polarized LEO SATCOM channels. Specifically, we maintain all other factors constant while varying XPD at 3 dB, 5 dB, and 12 dB [23]. We investigate changes in system throughput and QoS performance.

In Fig. 2, we define η as the ratio between the number of users whose QoS requirements are satisfied and the total users [8], which represents the QoS performance. In the dual-polarized LEO SATCOM channels, for each XPD, the value of η follows the same downward trend, which can be categorized into two stages. In particular, the value of η stays steady before reaching a certain threshold. It exhibits a gradual decline, with a progressively increasing rate of descent before reaching a certain threshold. Before that point, the QoS constraints are too small compared with the data rate and, thus, do not contribute to the performance of η. Note that increasing XPD can improve the signal to interference plus noise ratio (SINR) of received signals, thereby enhancing the QoS performance. However, the relationship between the XPD and η is nonlinear. When we gradually increase the XPD and it is relatively large, the matrix $\mathbf{X}$ in Eq. 2 approaches the identity matrix; thus, the change of η is rather small. Figure 3 compares the system throughput under different XPDs. The changing patterns of Figs. 2 and 3 exhibit remarkable similarity, with the underlying causal factors being almost identical.

Afterward, we conduct simulations to compare the performance of dual- and single-polarized MIMO SATCOM channels. The single-polarized MIMO SATCOM system has the same number of antennas with the dual-polarized antennas. The system model of the single-polarized channels is similar to that of [16,17,27].

Table 1. Simulation parameters

Parameter	Value
System bandwidth B_{w}	800 MHz
Carrier frequency	20 GHz
Rician factor κ_k	12 dB
Antenna gain G_{sat}, G_{ut}	3 dB
Satellite orbit altitude	1,000 km
Number of satellite antennas $N_{\text{t}}^{\text{x}}, N_{\text{t}}^{\text{y}}, N_{\text{t}}^{\text{d}}$	8, 8, 128
Number of UTs K	25
Number of time blocks	5

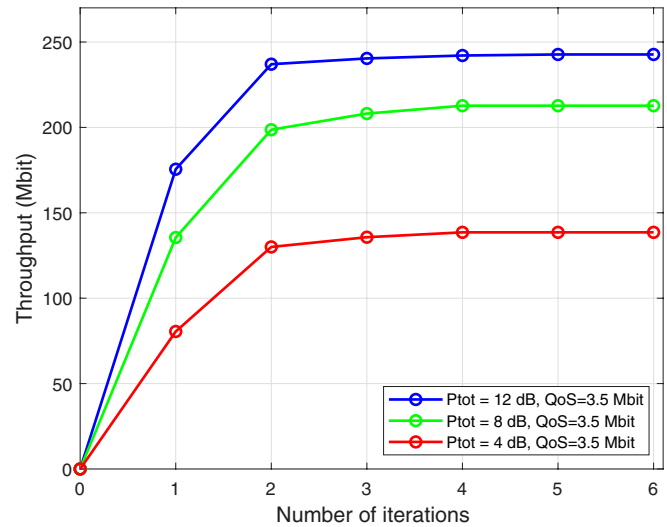

Fig. 1. Convergence performance versus the number of iterations.

In Fig. 4, η has the same definition with that in Fig. 2. Figure 5 evaluates the system throughput of dual- and single-polarized antennas, with respect to the QoS requirements. In particular, for different antenna types, the throughput follows the same downward trend, which can be categorized into 2 stages. It stays steady before reaching a certain threshold and exhibits a gradual decline, with a progressively increasing rate of descent. Note that the use of dual-polarized antennas in MIMO communication enables the simultaneous transmission and reception of signals in two different directions, resulting in increased system throughput. The changing patterns of Figs. 4 and 5 exhibit remarkable similarity, with the underlying causal factors being almost identical.

Finally, we conduct simulations to compare the performance between algorithms presented in this work and the max–min fairness precoding algorithm. The max–min fairness precoding algorithm, formulated as proportional fairness [3], aims to maximize the transmission rate of the worst user for fair distribution as follows

$$f = \underset{\mathbf{b}}{\text{maximize}} \ \underset{k,t}{\text{minimize}} \ R_k(\bar{t}). \tag{41}$$

Figure 6 shows the percentage of users achieving their QoS requirements, while Fig. 7 evaluates the system throughput of the proposed algorithm and the max–min fairness precoding algorithm, with respect to the QoS requirements. We set the $\eta = 0$ and Throughput $= 0$ when all users cannot achieve their QoS requirements. It can be noticed that the proposed algorithm shows significant improvement, compared with the max–min fairness framework. Meanwhile, from Fig. 6, note that when QoS rises to a certain threshold, the max–min fairness precoding algorithm will cause the majority of users to fail to meet their QoS requirements, resulting in a sharp drop in system throughput in Fig. 7.

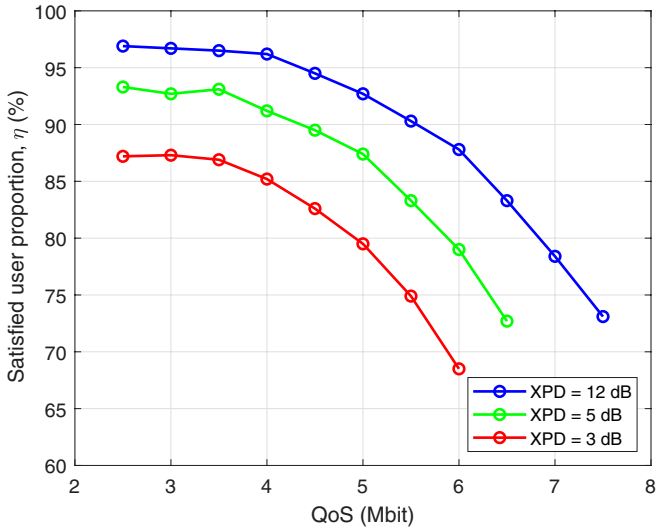

Fig. 2. Performance comparison between varying XPDs on satisfied user proportion.

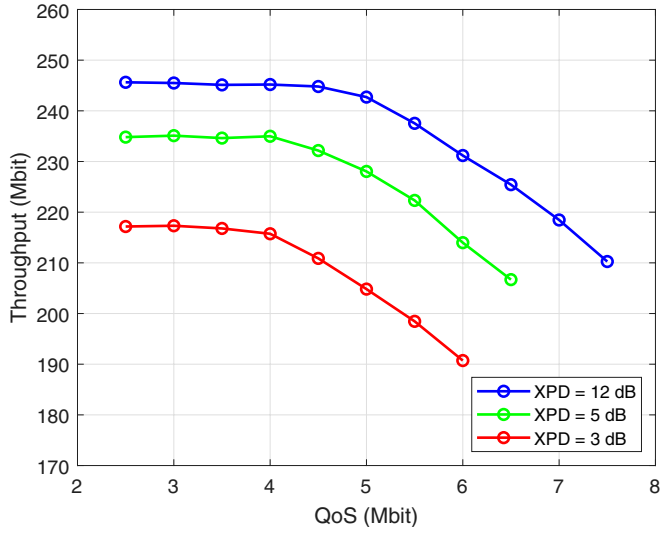

Fig. 3. Performance comparison between varying XPDs on system throughput.

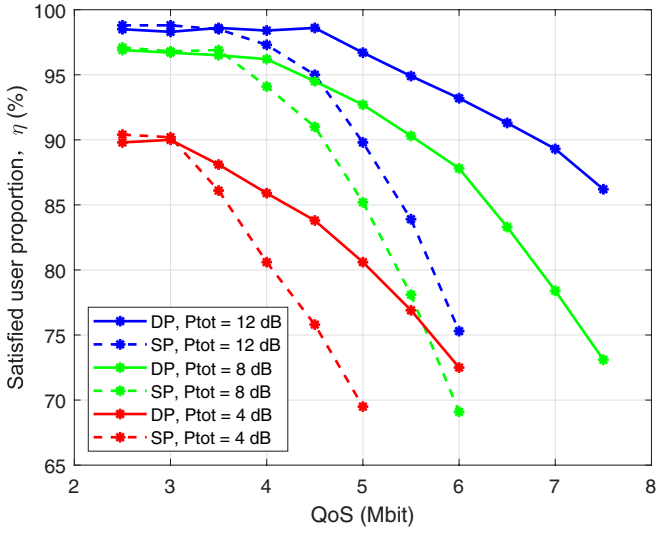

Fig. 4. Performance comparison between different antenna types on satisfied user proportion.

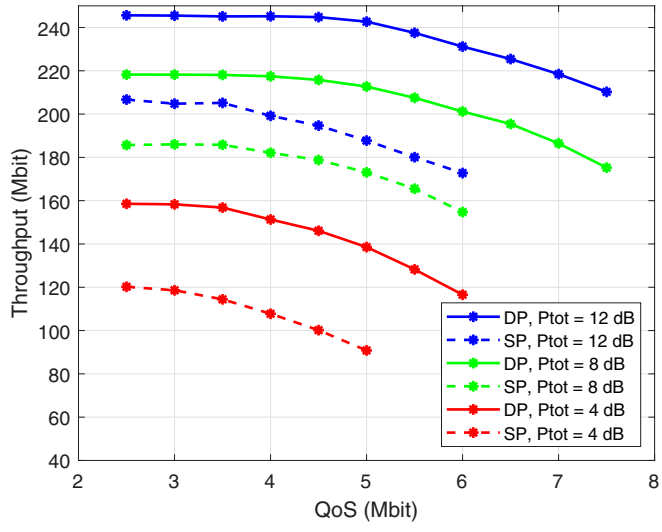

Fig. 5. Performance comparison between different antenna types on system throughput.

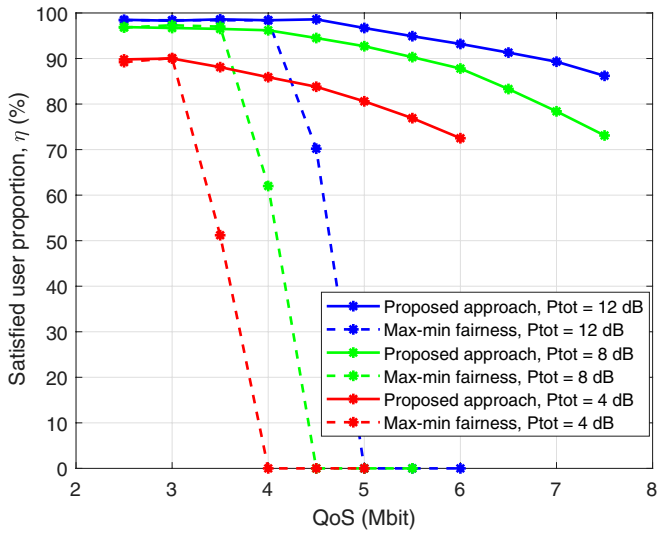

Fig. 6. Performance comparison between different algorithms on satisfied user proportion.

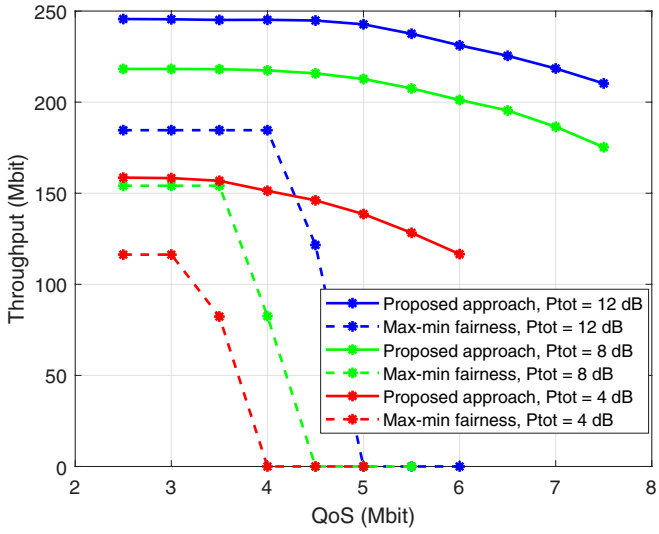

Fig. 7. Performance comparison between different algorithms on system throughput.

Conclusion

This study focused on optimizing the QoS-aware precoding design for the downlink massive MIMO LEO SATCOM. Through dual-polarized antenna technology, we jointly optimized the system throughput and QoS performance, accounting for slow-varying channel conditions. To tackle this problem, we proposed an algorithm consisting of two stages. In stage I, we employed iterative optimization with the Lagrange dual transform and proposed a user selection algorithm that ensures the QoS level of the majority of users. In stage II, we applied the WMMSE method and the block coordinate descent method to handle the precoding problem based on the results in stage I. Numerical results demonstrated that the proposed algorithm enables more users to achieve their QoS requirements, while the dual-polarized technology outperforms others in terms of system throughput.

Acknowledgments

Funding: This work was supported by the National Natural Science Foundation of China for Outstanding Young Scholars under grant 62322104, the Key Technologies R&D Program of Jiangsu (Prospective and Key Technologies for Industry) under grants BE2022067 and BE2022067-5, the Natural Science Foundation of Jiangsu Province under grant BK20231415, the Natural Science Foundation on Frontier Leading Technology Basic Research Project of Jiangsu under grant BK20222001, the Jiangsu Province Basic Research Project under grant BK20192002, and the Fundamental Research Funds for the Central Universities under grants 2242022k60007 and 2242023K5003.
Author contributions: Y. H. conducted the simulations and prepared the initial draft. L. Y. contributed to the idea, revisions, and suggestions. K. W. and X. G. contributed to reviewing, editing and reference searching.
Competing interests: The authors declare that they have no competing interests.

Data Availability

All data needed to evaluate the conclusions of the study are presented in the paper.

References

1. Fraire JA, Nies G, Gerstacker C, Hermanns H, Bay K, Bisgaard M. Battery-aware contact plan design for LEO satellite constellations: The ulloriaq case study. *IEEE Trans Green Commun Netw*. 2020;4(1):236–245.
2. Qu Z, Zhang G, Cao H, Xie J. LEO satellite constellation for Internet of Things. *IEEE Access*. 2017;5:18391–18401.
3. Zheng G, Chatzinotas S, Ottersten B. Generic optimization of linear precoding in multibeam satellite systems. *IEEE Trans Wirel Commun*. 2012;11(6):2308–2320.
4. You L, Li K-X, Wang J, Gao X, Xia X-G, Ottersten B. Massive MIMO transmission for LEO satellite communications. *IEEE J Sel Areas Commun*. 2020;38(8):1851–1865.
5. Gong S, Xing C, Chen S, Fei Z. Secure communications for dual-polarized MIMO systems. *IEEE Trans Signal Process*. 2017;65(16):4177–4192.
6. You L, Qiang X, Li K-X, Tsinos CG, Wang W, Gao X, Ottersten B. Hybrid analog/digital precoding for downlink massive MIMO LEO satellite communications. *IEEE Trans Wirel Commun*. 2022;21(8):5962–5976.
7. Huang Y, You L, Tsinos CG, Wang W, Gao X. QoS-aware precoding in downlink massive MIMO LEO satellite communications. *IEEE Commun Lett*. 2023;27(6):1560–1564.
8. Van Chien T, Lagunas E, Ta TH, Chatzinotas S, Ottersten B. User scheduling and power allocation for precoded multibeam high throughput satellite systems with individual quality of service constraints. *IEEE Trans Veh Technol*. 2022;72(1):907–923.
9. Liolis KP, Gómez-Vilardebó J, Casini E, Perez-Neira AI. Statistical modeling of dual-polarized MIMO land mobile satellite channels. *IEEE Trans Commun*. 2010;58(11):3077–3083.
10. Han Y, Li X, Tang W, Jin S, Cheng Q, Cui TJ. Dual-polarized RIS-assisted mobile communications. *IEEE Trans Wirel Commun*. 2022;21(1):591–606.

11. Paulraj A, Rohit AP, Nabar R, Gore D. *Introduction to space-time wireless communications* Cambridge (UK): Cambridge Univ. Press; 2003.
12. Oestges C, Clerckx B, Guillaud M, Debbah M. Dual-polarized wireless communications: From propagation models to system performance evaluation. *IEEE Trans Wirel Commun*. 2008;7(10):4019–4031.
13. Wallace J, Jensen M. Mutual coupling in MIMO wireless systems: A rigorous network theory analysis. *IEEE Trans Wirel Commun*. 2004;3(4):1317–1325.
14. Svantesson T, Ranheim A. Mutual coupling effects on the capacity of multielement antenna systems. Paper presented at: Proceedings of the 2001 IEEE International Conference on Acoustics, Speech, and Signal Processing; 2001 May 7–11; Salt Lake City, UT, USA.
15. Coldrey M. Modeling and capacity of polarized MIMO channels. Paper presented at: VTC Spring 2008—IEEE Vehicular Technology Conference; 2008 May 11–14; Marina Bay, Singapore.
16. Clerckx B, Craeye C, Vanhoenacker-Janvier D, Oestges C. Impact of antenna coupling on 2 × 2 MIMO communications. *IEEE Trans Veh Technol*. 2007;56(3):1009–1018.
17. Biswas S, Masouros C, Ratnarajah T. Performance analysis of large multiuser MIMO systems with space-constrained 2-D antenna arrays. *IEEE Trans Wirel Commun*. 2016;15(5):3492–3505.
18. Azam MA, Dutta AK, Mukherjee A. Performance analysis of dipole antenna based planar arrays with mutual coupling and antenna position error in mmWave hybrid system. *IEEE Trans Veh Technol*. 2021;70(10):209–221.
19. Garcia-Aguilar A, Inclan-Alonso J-M, Vigil-Herrero L, Fernandez-Gonzalez J-M, Sierra-Perez M. Low-profile dual circularly polarized antenna array for satellite communications in the X band. *IEEE Trans Antennas Propag*. 2012;60(5):2276–2284.
20. Bouhlel N, Saad M, Bader F. Sub-terahertz wireless system using dual-polarized generalized spatial modulation with RF impairments. *IEEE J Sel Areas Commun*. 2021;39(6):1636–1650.
21. Yin X, Gong S, Wang S, Zhang Z. Two timescale robust energy-efficient precoding for dual-polarized MIMO systems. *IEEE Trans Commun*. 2020;68(9):5575–5589.
22. Bui V-P, Van Chien T, Lagunas E, Grotz J, Chatzinotas S, Ottersten B. Robust congestion control for demand-based optimization in precoded multi-beam high throughput satellite communications. *IEEE Trans Commun*. 2022;70(10):6918–6937.
23. Lindmark B, Nilsson M. On the available diversity gain from different dual-polarized antennas. *IEEE J Sel Areas Commun*. 2001;19(2):287–294.
24. Zafari G, Koca M, Sari H. Dual-polarized spatial modulation over correlated fading channels. *IEEE Trans Commun*. 2017;65(3):1336–1352.
25. Kim S, Choi J, Song J. Beam designs for millimeter-wave backhaul with dual-polarized uniform planar arrays. *IEEE Trans Commun*. 2020;68(7):4202–4217.
26. Lindmark B. Comparison of mutual coupling compensation to dummy columns in adaptive antenna systems. *IEEE Trans Antennas Propag*. 2005;53(4):1332–1336.
27. Balanis CA. *Antenna theory: Analysis and design*. Hoboken (NJ): John Wiley & Sons Inc.; 2015.
28. Singh H, Sneha HL, Jha RM. Mutual coupling in phased arrays: A review. *Int J Antennas Propag*. 2013;2013:1–23.
29. Li K-X, You L, Wang J, Gao X, Tsinos CG, Chatzinotas S, Ottersten B. Downlink transmit design for massive MIMO LEO satellite communications. *IEEE Trans Commun*. 2022;70(2):1014–1028.
30. Wright SJ. *Primal-dual interior-point methods* Philadelphia (PA): SIAM; 1997.
31. Sun C, Gao X, Jin S, Matthaiou M, Ding Z, Xiao C. Beam division multiple access transmission for massive MIMO communications. *IEEE Trans Commun*. 2015;63(6): 2170–2184.
32. Pan C, Zhu H, Gomes NJ, Wang J. Joint precoding and RRH selection for user-centric green MIMO C-RAN. *IEEE Trans Wirel Commun*. 2017;16(5):2891–2906.
33. Shen K, Yu W. Fractional programming for communication systems—Part I: Power control and beamforming. *IEEE Trans Signal Process*. 2018;66(10):2616–2630.